Electrochimica Acta 276 (2018) 118–124

Contents lists available at ScienceDirect

Electrochimica Acta

journal homepage: www.elsevier.com/locate/electacta

Densely packed porous graphene film for high volumetric performance supercapacitor

Yuanzhi Chao [a], Songbo Chen [a], Huqiang Chen [a], Xinjun Hu [a], Yu Ma [a, b], Wensheng Gao [a], Yongxiao Bai [a, *]

[a] Institute of Material Science and Engineering, Key Laboratory for Magnetism and Magnetic Materials of the Ministry of Education, Key Laboratory of Special Function Materials and Structure Design of Ministry of Education, Lanzhou University, Lanzhou, 730000, China
[b] Department of Chemical Engineering and Biointerfaces Institute, University of Michigan, Ann Arbor, MI 48109-2136, United States

ARTICLE INFO

Article history:
Received 18 December 2017
Received in revised form
2 April 2018
Accepted 22 April 2018
Available online 23 April 2018

Keywords:
Porous graphene oxide
Film
Volumeric capacitance
Supercapacitor

ABSTRACT

Improving volumetric capacitance of supercapacitor is important and challenging for practical application. Here, porous graphene oxide (PGO) is prepared through an efficient method at room temperature after etched by $Zn(CH_3COO)_2$ in several minutes. The obtained densely packed porous graphene film (PGF) was constructed by a template-assisted method. And the perforated PGF electrode material exhibits a high volumetric capacitance (C_V) of 318.8 F cm^{-3} in 6.0 M KOH electrolyte at the current density of 1 A g^{-1}. In addition, it exhibited excellent cycling stability, that is 88% retention of capacitance after 10000 charge/discharge cycles in the current density of 5 A g^{-1}. Furthermore, it demonstrates a capacitance of 219.0 F cm^{-3} (1 A g^{-1}) and a cycling stability of 113% (10000 charge/discharge cycles at 5 A g^{-1}) after assembled into symmetric supercapacitor. So the PGF is promising to be applied in the high performance energy storage devices with lighter quality and smaller volume.

1. Introduction

Graphene, a single layer of carbon hybridized by sp^2, has been researched in various fields due to its excellent physical, chemical, mechanical properties. Recently, the graphene based supercapacitors have been extensive researched due to the good electrical conductivity of 10^8 S m^{-1} [1], a large theoretical specific surface area (2630 m^2 g^{-1}) [2,3] and a high theoretical capacitance of about 550 F g^{-1} [4,5]. But there are obvious drawbacks when the graphene directly used as the electrode materials, such as the few electrolyte ion transport channels caused by the agglomerating and restacking of graphene or graphene oxide [6,7]. Which makes the electrochemical performance of the graphene based supercapacitor inferior to the theoretical value, further hindering its development in practical application. In order to meet the demands of high electrochemical performance as electrode materials, graphene has been focused on the optimization in structure and properties, such as architectural design [8–13], doped elements modification [14–17] and hole etching [18]. Above micropores and mesopores structure design provide the larger specific surface area (SSA) for charge adsorption and more ion fast transporting channel, further realize the high capacitance under large current density [19]. In addition, these nanopores on the in-planes of graphene sheets provide more edging sites to form electrical double layers [20]. Therefore, the appropriate layer spacing and the porous structure are the key factors to fabricate the high performance capacitance.

Therefore, the porous graphene (PG), one of the result of graphene modification, has been widely studied to solve some drawbacks of graphene based electrode materials and realize the high capacitance performance. It can be prepared by many methods, such as reduction of PGO obtained by graphene oxide (GO) etching [21,22], carbonization of carbonaceous materials [23] and exfoliation of holy graphite oxide [21]. Commonly, these methods need heat treatment, strong acid and a longer synthesis time [21,22,24,25]. All of these shortcoming of above PG synthesis methods has brought a huge obstacle to its practical application and development. On the other hand, energy storage devices, such as battery and supercapacitor, prefer to be designed to be relatively lighter and smaller when applied in all kinds of machinery and equipment in actual industry. Thus, to solve above problems, higher density electrode materials are required gradually in practical

* Corresponding author.
E-mail address: baiyx@lzu.edu.cn (Y. Bai).

https://doi.org/10.1016/j.electacta.2018.04.156
0013-4686/

application. However, to date, the common porous carbon materials with high gravimetric capacitance (C_g) always have the same problem, lower bulk densities of less than 0.5 g cm^{-3} during maintaining high porosity [19], determining the lower C_V. For example, Shao, Y. et al. promoted the C_g of 3D porous graphene films by combining freeze casting and filtration, but could not ensure the high density (only 0.23 g cm^{-3}) [9]. So that the devices assembled by these lower density materials possess heavier mass and larger volume. Such supercapacitors obtaining high C_g but low C_V, as energy storage, cannot meet with the actual application and requirement. The key issue here is the efficient combination of both excellent C_g and C_V caused by densely packed electrode materials with ample electrically conductive channels and appropriate pseudocapacitive functional groups at the same time.

Despite the variety of the construction methods, the challenges with their universality to create uniform porous geometries and densely packed graphene film electrode exhibiting a high volumetric capacitance still remain. To solve these above mentioned problems, a rapid and facile method is explored and used to prepare the PG in this work. Herein, we have investigated a densely packed porous electrode material (PGF) with graphene from hydrothermal process. The PGF exhibited a lighter quality and smaller volume due to the porosity and high density, which can bring high C_g and C_V to the supercapacitor. Firstly, GO is mixed with $Zn(CH_3COO)_2$ in room temperature without other water-insoluble produced within several minutes. PGO and small GO (fragments coming from PGO) are produced by washing with HCl. The rapid preparation of PGO can be also used to prepare graphene quantum dots (GQDs) by over-etching in a longer time. After that, we create a film of $Zn(OH)_2$/ZnO(Z)/graphene/Z/graphene/Z, and Z acts as the "spacers" in such heterostructure. The densely packed PGF as the final product is achieved by removing Z subsequently. The $Zn(CH_3COO)_2$ etching process of GO is quickly with just several minutes, and the pore size is uniform and controllable. The resulting porous graphene films (PGF2-10) possesses a high density of 1.335 g cm^{-3}, exhibits a C_g of 238.7 F g^{-1} and a C_V of 318.8 F cm^{-3} in three-electrode system at 1 A g^{-1}. The symmetrical device assembled with PGF2-10 also exhibits a C_g of 164.4 F g^{-1} and a C_V of 219.0 F cm^{-3} in an aqueous electrolyte of 6.0 M KOH. It demonstrates that such graphene films are promising to be used in the lighter energy storage device.

2. Results and discussion

The schematic illustration for the fabrication of PGO, porous graphene/Z composite films (PGZF) and PGF is shown in Scheme 1. The experiment process was described as follows. Firstly, $Zn(CH_3COO)_2$ aqueous solution was added into GO homogeneous solution under stirring, then PGO-contained mixed solution was get several minutes later. The PGO with different porosity degree was obtained successively by configuring above mixed solution with HCl and deionized water. The thickness of GO and PGO10 are ~0.9 nm as shown in the AFM images of Scheme 1 and Fig. S1, respectively. Which suggests the sheets of GO and PGO are absolutely dispersed in aqueous solution. Some small sheets with dozens of nanometers stacked on the sheets of PGO10 (Fig. S1), this phenomenon came from the effect of hole etching, corresponding to Fig. 1(a and b). The etching may derived from the activation of $ZnCl_2$ [26,27]. If the above GO, templating agent and reductant mixed solution experiencing chemical reduction, the graphene/Z mixed solution was formed, in which Z gained from the reaction between $Zn(CH_3COO)_2$ and OH. OH was derived from $N_2H_4 \cdot H_2O$ and $NH_3 \cdot H_2O$ served as the reductant and stabilizer, respectively. The PGZF was achieved by means of vacuum filtrating the graphene/Z mixture, Z of the film performed as "spacers" between the two sheets of graphene to prevent sheets agglomerating during the dry contraction. The porous structure of film was self-supported after drying, and maintained after moving Z "spacers" using 10 wt % HCl. The sandwich structure of PGZF (Scheme 1 and the inset of Fig. S2) is similar to ZnO-spaced graphene [5] and rGO-IL/SiO_2 spheres [28], Compared with them, our strategy is more simple and rapid. The density of PGF compassed is around 1.335 g cm^{-3} evaluated. Fig. S4 is the optical images of PGZF and PGF with a certain flexibility.

2.1. Morphology and structure

As shown in Fig. 1, compared with GO (Fig. 1a), the nanopores are well-distributed on the platelets of PGO2 (Fig. 1b), PGO10 (Fig. 1c) and PGO60 (Fig. 1d), the surface of these platelets are neat and smooth. In addition, PGO10 exhibits a predominantly disordered structure with abundant micropores and mesopores (Fig. 1c). The amorphous structure can be clearly seen from the high-

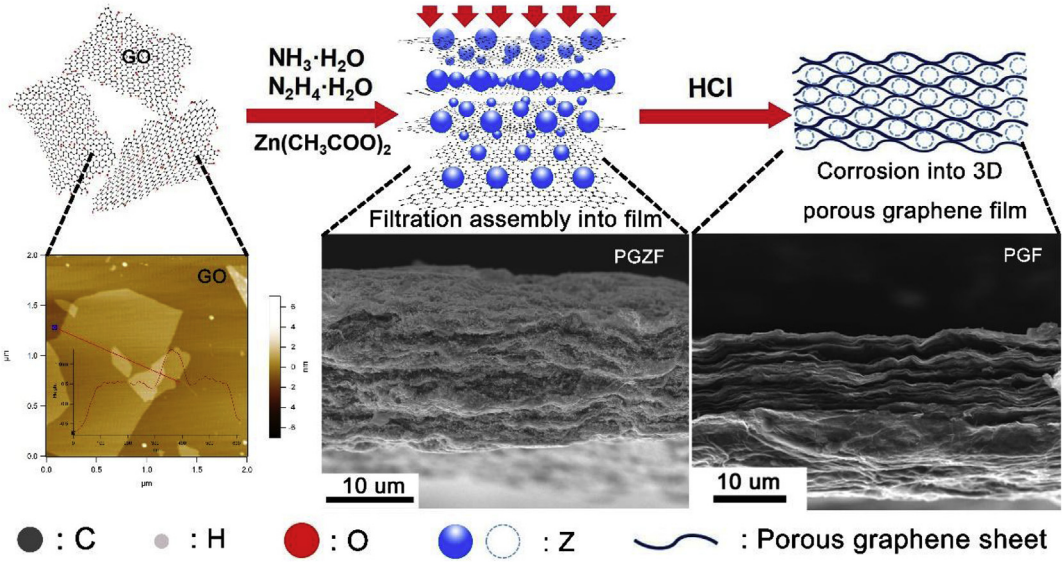

Scheme 1. The preparation of PGZF and PGF.

resolution TEM image of PGO10 as shown in the inset of Fig. 1c. In addition, this porous structure could be still remained after reduced into graphene (Fig. S5). Notably, these micro-mesopores are benefit to the adsorption/desorption of the charge and the transport and diffusion of the electrolyte ion [29,30], so as to enhance the rate capability performance especially in rapid charge/discharge at large current densities. The PGO60 was seriously etched as shown in Fig. 1d, the sheets of PGO60 trend to be broken into pieces with few nanometers. Therefore, this method is promising to be applied in the green and rapid synthesis of GQDs. The large holes on the sheets of PGO2 (Fig. 1b) may be caused by the pores etching, and some parts of large sheets were cut into small sheets with few tens of nanometers. Which is also supported by the AFM characterization as shown in Fig. S1.

The structure changing was further characterized by the XRD. The sharp peak of PGZF2-10 (Fig. 2a) correspond to the $Zn(OH)_2$ and ZnO by contrasting with the PDF cards of PDF#38-0385 ($Zn(OH)_2$) and PDF#36-1457 (ZnO). The existence of Zn element also was demonstrated in the EDS (Fig. S2) and XPS (Fig. S3). The broad peak center of PGZF2-10 in about 22.3° of two theta position correspond to the (002) contrasted with the GO. In the meanwhile, the sharp peak ($2\theta = 10.1^\circ$) of the GO disappeared in the PGZF2-10, revealing that the Z particles were successfully inserted into the graphene layers and the GO in PGZF was successfully reduced [31]. The peaks ($2\theta = 12.5^\circ$, 22.3°) of PGF2-10 shifted to lower angle compared to that of GF ($2\theta = 16.5^\circ$, 22.6°) caused by the porous supported structure, indicating less ordering of graphitic layers and a larger interlayer distance of graphene sheets [32]. The weak peak (~13.5° of GF and ~12.5° of PGF2-10) derived from the exist of the residual oxygen containing functional groups which hindering graphene sheets stack and further increasing the interlayer spacing. Giving to the central position of (002) peak in PGF2-10 (22.3°) gained from PGZF2-10, had not been lower compared with that of PGZF ($2\theta = 22.5^\circ$), combined with the disappearance of Z demonstrated on Fig. 2a and Fig. S3, we suggest that the "spacers" (Z) supported the hole between graphene sheets, and these holes are not aggregated after removing these "spacers".

The structure and reduction degree of as-prepared samples were also characterized by Raman spectroscopy (Fig. 2b). The D band is associated with disordered carbonaceous structure or graphene edges [33], while the G band is ascribed to the vibration of all sp^2 hybridized carbon atoms in both rings and chains [16]. The GO have a higher intensity G band at ~1600 cm^{-1} compared with the D band at about 1350 cm^{-1}, and the I_D/I_G ratio is 0.97. But the intensity of the D band is higher than the G band in the GF and PGF2-10. The I_D/I_G ratio increases from 0.97 of GO to 1.05 (GF) and 1.03 (PGF2-10)

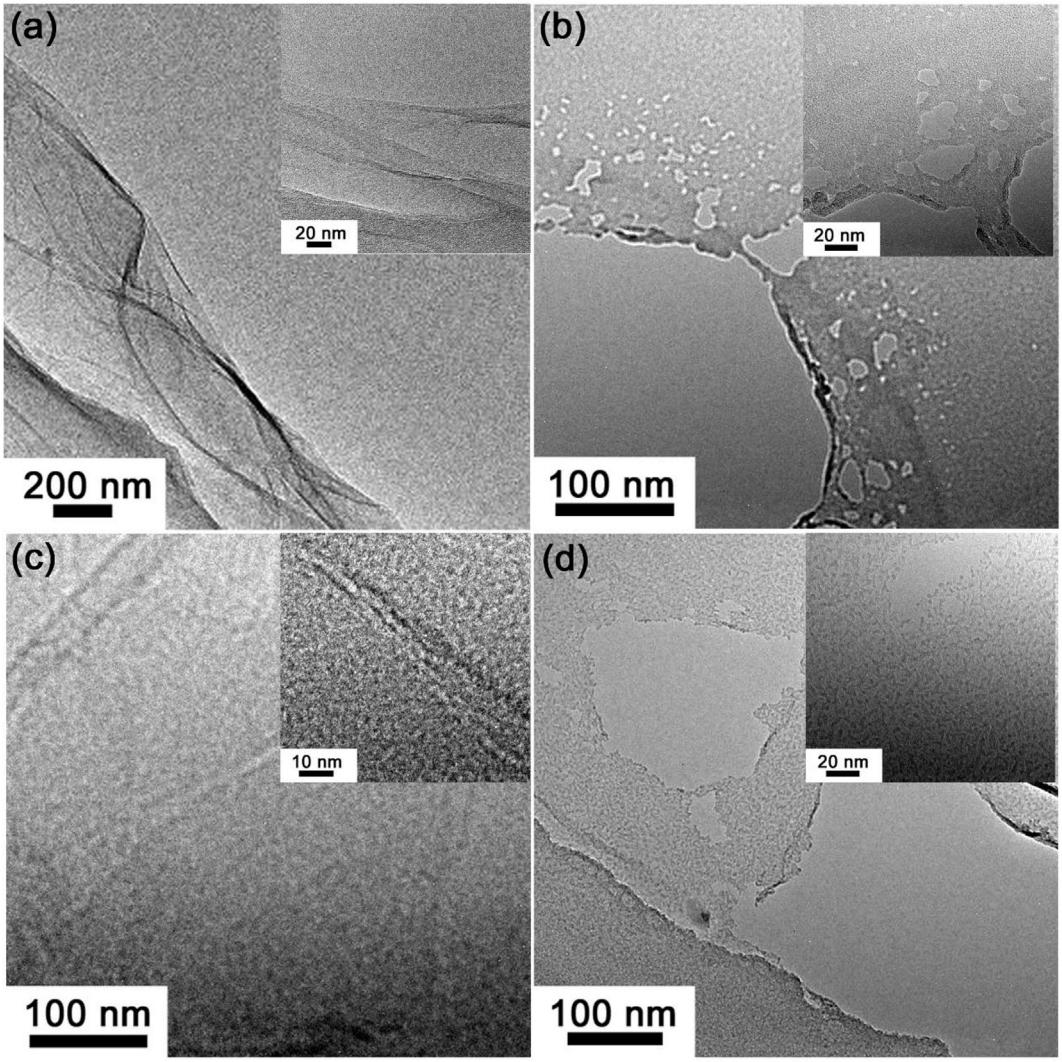

Fig. 1. Low and high magnification TEM images of **(a)** GO, **(b)** PGO2, **(c)** PGO10 and **(d)** PGO60.

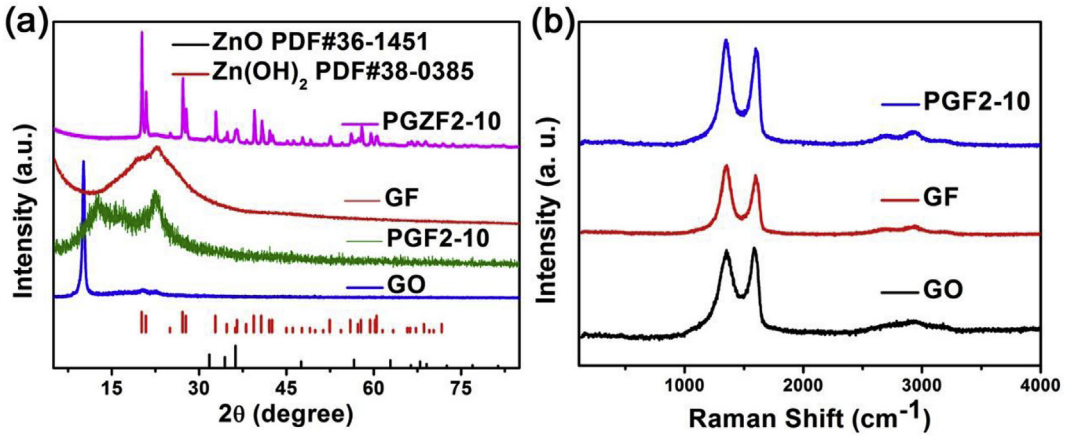

Fig. 2. **(a)** XRD and **(b)** Raman of samples.

respectively, indicating that the chemical reduction of oxygen containing functional groups and the etching of holes increased the amount of lattice defects [30,34]. Pores produced a relatively abundant graphene edges, which decreasing the proportion of sp^2, so as to make porous graphene possesses higher I_D/I_G than GF without high porosity. But the above inference is in an opposite of the result of the actual I_D/I_G results. The reason why the I_D/I_G ratio of PGF2-10 lower than GF in fact may be that the reduction degree of PGF2-10 was lower than GF [35]. Comparing with GF, the lower reduction degree of PGF2-10 also can be demonstrated by the lower C/O of PGF2-10 than GF in Fig. 4 and Table S1.

The element composition and surface chemical structure of samples are shown in Fig. 3 and Fig. S3. Fig. 3a suggest that the as prepared GF and PGF2-10 contain C and O as the main elements, resulting that the C/O is about 4.197 and 3.099 respectively, all lower than that of GO (C/O = 2.723) [36]. The detailed element content and the composition of chemical bonds are listed in Table S1. The intensity of C-O (12.63%) and C=O (3.83%) were significantly weaker than C-C/C=C (83.54%) in GF (Fig. 3c), suggesting that oxygen containing groups may be consumed in the process of reduction. But for the PGF2-10, different from GF, retained abundant C-O (36.94%) which derived from lower

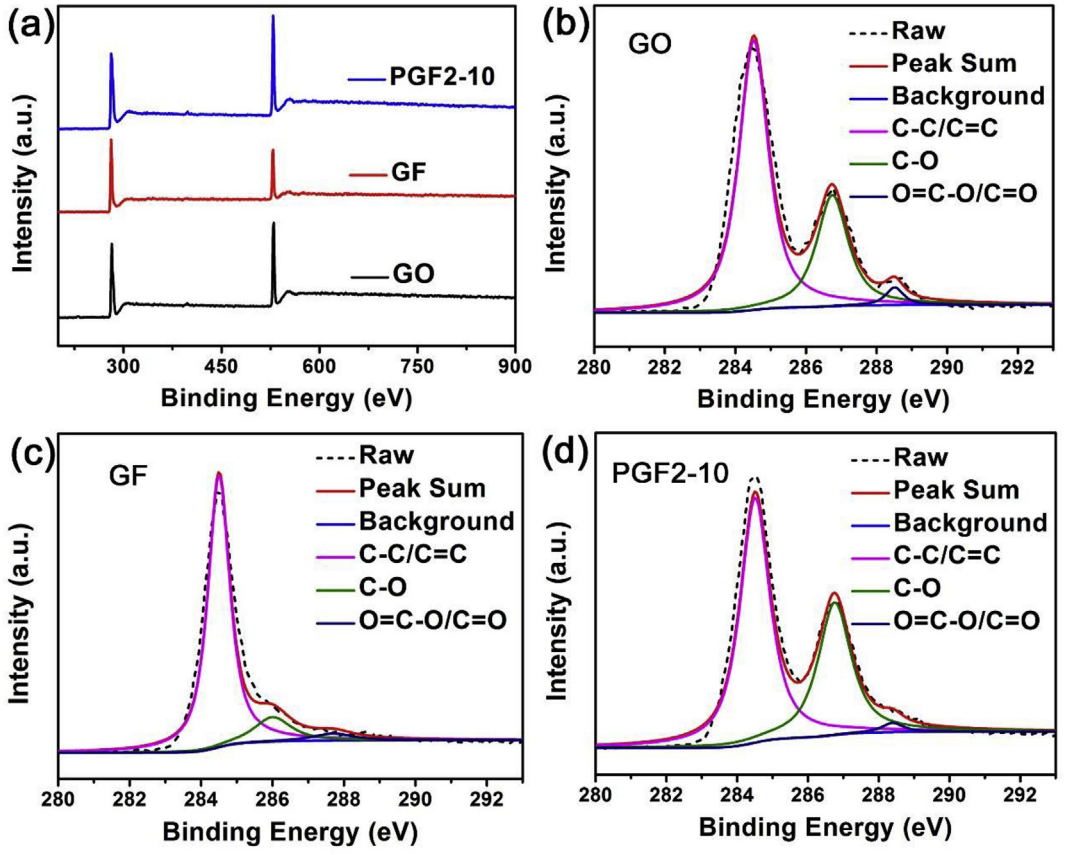

Fig. 3. **(a)** The XPS and **(b, c and d)** High-resolution C 1s spectra of samples.

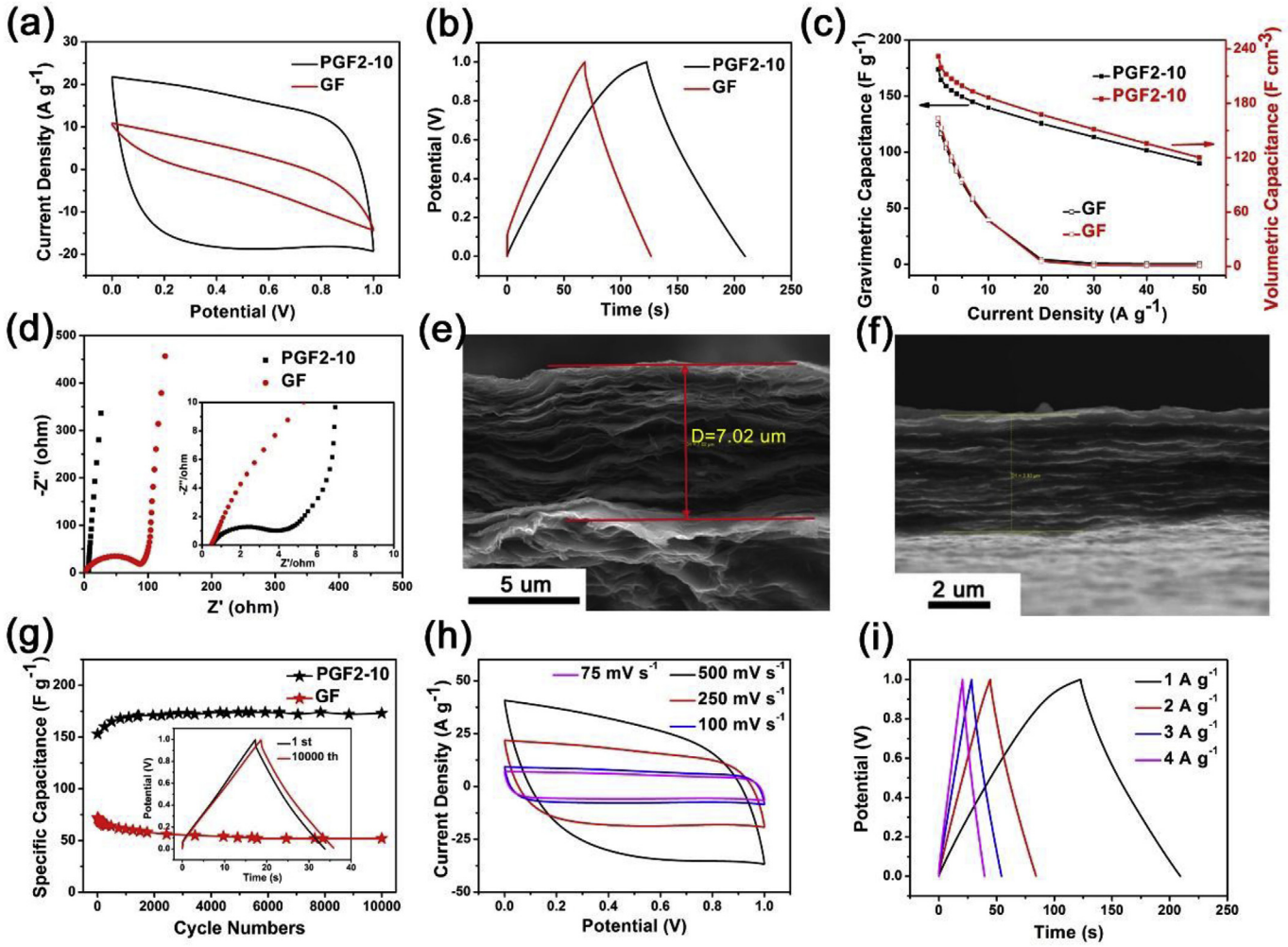

Fig. 4. Two-electrode system: **(a)** CV curves of samples at scan density of 250 mV s^{-1}, **(b)** GCD curves of samples at current density of 1 A g^{-1}, **(c)** C_g and C_V and **(d)** Nyquist plot of samples, **(e)** SEM image of the PGF2-10 cross section and **(f)** SEM image of the GF cross section, **(g)** Cycling stability of samples in two-electrode system (the inset is the GCD curve of PGF2-10), **(h)** CV and **(i)** GCD curves of PGF2-10.

reduction and higher porosity. The functional group of C-O will be able to increase wettability and afford pseudocapacitance [37,38] which corresponding to the properties of electrochemistry (Fig. S7).

2.2. Electrochemical performance

The electrochemical performance of materials were investigated by electrochemical test in three and two electrode system. The materials was divided into two pieces with the same mass as the negative and positive electrode without any binders and additives to assemble a symmetric supercapacitor. To evaluate the capacitive properties of samples, Series of electrochemical properties and other evaluations were performed as follows.

In the two-electrode system, the area of CV curves (Fig. 4a) of PGF2-10 is larger than that of GF, revealing the larger C_g of PGF2-10. And the CV curve of PGF2-10 shows a greater rectangular shape, suggesting lower equivalent series resistances (ESR) [39]. Moreover, the shape of the CV profile GF became more distorted at 100 mV s^{-1}, suggesting that the diffusion of electrolyte ion was less effective [39,40], contributed to the lower porosity and the higher electrolyte resistance compared to PGF2-10 [41]. The drain voltage at charge curve and the voltage drop (IR) at discharge curve of GF can be seen obviously in contrast with PGF2-10 (Fig. 4b), indicating the excellent current response characteristic of PGF2-10. C_g and C_V versus current densities for samples in two-electrode system are supplied in Fig. 4c. In which, the capacitance of PGF2-10 evaluated by GCD curves are 164.4 F g^{-1} and 219.0 F cm^{-3}, higher than that of GF (116.4 F g^{-1} and 152.7 F cm^{-3}). The capacitances of PGF2-10 and GF retain 54.7% and 0.5% of initial capacitance respectively when the current density increase from 1 A g^{-1} to 50 A g^{-1}. Such a high C_V comes from high bulk density of PGF2-10. Furthermore, the capacitance can be remained effectively with 139.6 F g^{-1} and 186.4 F cm^{-3} at 10 A g^{-1} when the current density increases gradually. The porosity and conductivity occupy the important position in those factors affecting the performance of electrode materials. The properties of samples in three-electrode system are demonstrated in the supporting information (Fig. S7). PGF2-10 possesses high Cg (224.9 F g^{-1}) and C_V (318.8 F cm^{-3}) in 6.0 M KOH electrolyte at the current density of 1 A g^{-1} and low ESR. Fig. 4d reveals the EIS of samples in two-electrode system, similar with samples in three-electrode system displayed in Fig. S7e. The R_{ct} (~3.4 Ω), Warburg impedance and ESR (~6.6 Ω) of PGF2-10 are all visibly lower than that of GF, besides the R_s that PGF2-10 and GF have a similar R_s (~0.6 Ω). The EIS differences between PGF2-10 and GF greatly illustrate that these pores in graphene sheets are benefit to the diffusion and transport of ion and charge [42].

The impact of the graphene sheets packing way to the film structure showed in the SEM images of cross section. PGF2-10 (Fig. 4e) was more tousier than GF (Fig. 4f). The graphene sheets stacked and connect with each other with little spaces between sheets, while the GF demonstrates an agglomerate state. On the structure of PGF2-10, these spaces between sheets acted as horizontal channel, cooperating in-plan pores acted as vertical channel, a connected three-dimensional network was formed and used as paths to transfer electrolyte ion. However, as for the GF, electrolyte was difficult to diffuse from the surface to the interior when used as electrode materials due to without pores to get accessed to on the sheets of graphene. The specific surface area and pore structure (Fig. S6) illustrate that the effect of compressing the PGF2-10 with 10 MPa stress was to decrease macropore proportion and make some mesopore turn into micropore [19,43]. Compressing makes films become more compact so as to improve the C_V without large negative effect to the C_g.

In the three electrode system, the capacitance retention (Fig. S8) of PGF2-10 and GF are ~88% and ~77% of their initial capacitance, respectively. And the GCD curves maintain triangular shape after cycling. In the two electrode system, the capacitance retention (Fig. 4g) of PGF2-10 and GF remained about 113% and 72% after 10000 charge-discharges at a current density of 5 A g^{-1}. It is worth noting that the increased capacitance of PGF2-10 in the beginning of cycle is due to the gradual infiltration of electrolyte to the electrode materials in the charge-discharge processes. Infiltration makes the wettability of the electrode materials to the electrolyte becomes better [44,45]. The GCD curves without large change before and after 10000 cycles was displayed in the inset of Fig. 4g, implying the long-term electrochemical stability. The CV curves of PGF2-10 still maintain a rectangular shape without any distortion even at a high scan rate of 250 mV s^{-1} (Fig. 4h), also revealing small ESR. These GCD curves of PGF2-10 at different current density show a symmetrically triangular except for the curve at current density of 1 A g^{-1} (Fig. 4i), suggesting an ideal electrical-double-layer capacitive behavior.

In order to optimize the electrode materials performance, samples with different etching degree controlling by string time and proportion of $Zn(CH_2COO)_2$ were measured (the supported information). As a result, the best sample is PGF2-10, which demonstrated that the electrode materials should have a certain pore distribution but not the bigger pores is the better for the excellent electrochemical performance [43].

Accordingly, the PGF2-10 delivered an high C_g of 238.7 F g^{-1}, much higher than the graphene films [46,47] even some of N elements-doped graphene films [33]. Furthermore, the PGF2-10 exhibited a significant C_V of 318.8 F cm^{-3} at 1 A g^{-1}, superior than 3D-PGF with structure design [6,48]. And the electrode materials loading can reach 0.937 mg cm^{-2}. The detail was shown in the supported information (Table S2). These results further demonstrated the essential merits of the porous structure films for the light energy storage.

3. Conclusions

In summary, we report a rapid, facile and convenient chemical approach for preparing PGO in neutral solution at room temperature, the pores etching processes need 2–10 min. The pores on the surface of PGO could be controllably got by optimizing the reaction condition. We also develop a densely packed PGF2-10 electrode materials with high gravimetric and volumetric capacitance of ~238 F g^{-1} and ~318 F cm^{-3} (at a current density of 1 A g^{-1}), respectively. Two electrode symmetrical coin cell of PGF2-10 also obtains the great cycle stability (113% capacitance retention at 5 A g^{-1} after 10000 cycles). This method can also be used to produce GQDs by over-etching. It is promising to be applied in the flexible, light and high performance supercapacitors.

Appendix A. Supplementary data

Supplementary data related to this article can be found at https://doi.org/10.1016/j.electacta.2018.04.156.

References

[1] H. Wu, Y. Zhang, L. Cheng, L. Zheng, Y. Li, W. Yuan, X. Yuan, Energy Storage Mater. 5 (2016) 8–32.
[2] Q. Li, X. Guo, Y. Zhang, W. Zhang, C. Ge, L. Zhao, X. Wang, H. Zhang, J. Chen, Z. Wang, L. Sun, J. Mater. Sci. Technol. (2017) 793–799.
[3] L. Hu, X. Peng, Y. Li, L. Wang, K. Huo, L.Y.S. Lee, K.Y. Wong, P.K. Chu, Nano Energy 34 (2017) 515–523.
[4] Z.-S. Wu, Y. Zheng, S. Zheng, S. Wang, C. Sun, K. Parvez, T. Ikeda, X. Bao, K. Müllen, X. Feng, Adv. Mater. 29 (2017) 1602960–1602967.
[5] Y. Guo, B. Chang, T. Wen, C. Zhao, H. Yin, Y. Zhou, Y. Wang, B. Yang, S. Zhang, RSC Adv. 6 (2016) 19394–19403.
[6] Y. Bai, X. Yang, Y. He, J. Zhang, L. Kang, H. Xu, F. Shi, Z. Lei, Z.-H. Liu, Electrochim. Acta 187 (2016) 543–551.
[7] G.A. Ferrero, M. Sevilla, A.B. Fuertes, Sustain. Energy Fuels 1 (2017) 127–137.
[8] L. Zhang, C. Yang, N. Hu, Z. Yang, H. Wei, C. Chen, L. Wei, Z.J. Xu, Y. Zhang, Nano Energy 26 (2016) 668–676.
[9] Y. Shao, M.F. El-Kady, C.W. Lin, G. Zhu, K.L. Marsh, J.Y. Hwang, Q. Zhang, Y. Li, H. Wang, R.B. Kaner, Adv. Mater. 28 (2016) 6719–6726.
[10] Q. Wang, J. Yan, Z. Dong, L. Qu, Z. Fan, Energy Storage Mater. 1 (2015) 42–50.
[11] Y. Song, J. Yang, K. Wang, S. Haller, Y. Wang, C. Wang, Y. Xia, Carbon 96 (2016) 955–964.
[12] U.N. Maiti, J. Lim, K.E. Lee, W.J. Lee, S.O. Kim, Adv. Mater. 26 (2014) 615–619, 505.
[13] S.H. Lee, H.W. Kim, J.O. Hwang, W.J. Lee, J. Kwon, C.W. Bielawski, R.S. Ruoff, S.O. Kim, Angew. Chem. 49 (2010) 10084–10088.
[14] Y. Yu, J. Du, L. Liu, G. Wang, H. Zhang, A. Chen, J. Nanoparticle Res. 19 (2017), 191–131.
[15] J. Li, G. Zhang, C. Fu, L. Deng, R. Sun, C.-P. Wong, J. Power Sources 345 (2017) 146–155.
[16] G. Ma, Z. Zhang, H. Peng, K. Sun, F. Ran, Z. Lei, J. Solid State Electrochem. 20 (2016) 1613–1623.
[17] X. Wang, G. Sun, P. Routh, D.H. Kim, W. Huang, P. Chen, Chem. Soc. Rev. 43 (2014) 7067–7098.
[18] D. Wang, S. Liu, L. Jiao, G. Fang, G. Geng, J. Ma, Carbon 119 (2017) 30–39.
[19] S. Murali, N. Quarles, L.L. Zhang, J.R. Potts, Z. Tan, Y. Lu, Y. Zhu, R.S. Ruoff, Nano Energy 2 (2013) 764–768.
[20] Q. Zhou, M. Zhang, J. Chen, J.D. Hong, G. Shi, ACS Appl. Mater. Interface. 8 (2016) 20741–20747.
[21] Y. Zhang, L. Ji, W. Li, Z. Zhang, L. Lu, L. Zhou, J. Liu, Y. Chen, L. Liu, W. Chen, Y. Zhang, J. Power Sources 334 (2016) 104–111.
[22] S.K. Singh, V.M. Dhavale, R. Boukherroub, S. Kurungot, S. Szunerits, Appl. Mater. Today (2016) 141–149.
[23] Y. Hao, F. Xu, M. Qian, J. Xu, W. Zhao, F. Huang, RSC Adv. 7 (2017) 10901–10905.
[24] J. Xu, G. Wang, J. Cao, Y. Xue, Y. Li, W. Wang, Z. Chen, Ionics 22 (2016) 1177–1184.
[25] H. Zhao, J. Wang, D. Zhang, Q. Dai, Q. Han, P. Du, C. Liu, Y. Xie, Y. Zhang, H. Cao, Z. Fan, Sci. Rep. 7 (2017) 42643–42744.
[26] X. He, P. Ling, J. Qiu, M. Yu, X. Zhang, C. Yu, M. Zheng, J. Power Sources 240 (2013) 109–113.
[27] Q. Xie, A. Zheng, S. Zhai, S. Wu, C. Xie, Y. Zhang, Y. Guan, J. Solid State Electrochem. 20 (2015) 449–457.
[28] T. Li, N. Li, J. Liu, K. Cai, M.F. Foda, X. Lei, H. Han, Nanoscale 7 (2015) 659–669.
[29] Z. Li, D. Li, Z. Liu, B. Li, C. Ge, Y. Fang, Electrochim. Acta 158 (2015) 237–245.
[30] W. Yang, W. Yang, F. Ding, L. Sang, Z. Ma, G. Shao, Carbon 111 (2017) 419–427.
[31] W. Tian, Q. Gao, Y. Tan, Z. Li, Carbon 119 (2017) 287–295.
[32] S. Wu, G. Chen, N.Y. Kim, K. Ni, W. Zeng, Y. Zhao, Z. Tao, H. Ji, Z. Lee, Y. Zhu, Small 12 (2016) 2376–2384.
[33] M. Kota, X. Yu, S.-H. Yeon, H.-W. Cheong, H.S. Park, J. Power Sources 303 (2016) 372–378.
[34] B. Wang, Y. Qin, W. Tan, Y. Tao, Y. Kong, Electrochim. Acta 241 (2017) 1–9.
[35] Z.-Q. Hao, J.-P. Cao, Y. Wu, X.-Y. Zhao, Q.-Q. Zhuang, X.-Y. Wang, X.-Y. Wei, J. Power Sources 361 (2017) 249–258.
[36] X. Ye, Y. Zhu, Z. Tang, Z. Wan, C. Jia, J. Power Sources 360 (2017) 48–58.
[37] G. Lota, E. Frackowiak, Fuel Cell. 10 (2010) 848–855.
[38] F. Liu, D. Xue, Chemistry 19 (2013) 10716–10722.
[39] V.H. Pham, J.H. Dickerson, J. Phys. Chem. C 120 (2016) 5353–5360.
[40] J. Jiang, L. Bao, Y. Qiang, Y. Xiong, J. Chen, S. Guan, J. Chen, Electrochim. Acta 158 (2015) 229–236.
[41] D. Puthusseri, V. Aravindan, S. Madhavi, S. Ogale, Energy Environ. Sci. 7 (2014) 728–735.
[42] M. Amirhoseiny, M. Zandi, A. Mosayyebi, M. Khademian, Mod. Phys. Lett. B 30

(2016), 1550272–1550278.
[43] Y. Bu, T. Sun, Y. Cai, L. Du, O. Zhuo, L. Yang, Q. Wu, X. Wang, Z. Hu, Adv. Mater. 29 (2017) 1700470–1700477.
[44] J. Jiang, H. Chen, Z. Wang, L. Bao, Y. Qiang, S. Guan, J. Chen, J. Colloid Interface Sci. 452 (2015) 54–61.
[45] W. Chen, C. Xia, H.N. Alshareef, Nano Energy 15 (2015) 1–8.
[46] L. Jiang, L. Sheng, C. Long, Z. Fan, Nano Energy 11 (2015) 471–480.
[47] M. Wang, D. Duong le, N.T. Mai, S. Kim, Y. Kim, H. Seo, Y.C. Kim, W. Jang, Y. Lee, J. Suhr, J.D. Nam, ACS Appl. Mater. Interface. 7 (2015) 1348–1354.
[48] C.Z. Yuan, L. Zhou, L.R. Hou, Mater. Lett. 124 (2014) 253–255.